Electronic Supplementary Material (ESI) for Journal of Materials Chemistry A.

Supporting Information

Interface Engineering with AlO_x dielectric layer enabling an ultrastable Ta_3N_5 photoanode for photoelectrochemical water oxidation

Yongle Zhao[a, b], Guiji Liu[a, b], Hong Wang[a, b], Yuying Gao[a,b], Tingting Yao[a], Wenwen Shi[a, b], Can Li*[a]

a. State Key Laboratory of Catalysis, Dalian Institute of Chemical Physics, Chinese Academy of Sciences, Dalian National Laboratory for Clean Energy, Zhongshan Road 457, Dalian 116023, P. R. China. E-mail: canli@dicp.ac.cn

b. University of Chinese Academy of Sciences, Beijing 100049, P. R. China

*Corresponding author. E-mail address: canli@dicp.ac.cn (Prof. Can Li)

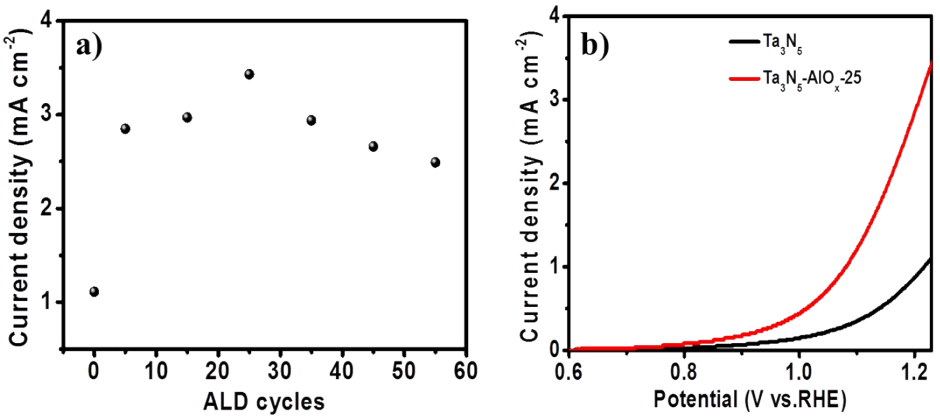

Fig. S1 a) Current density of Ta_3N_5 photoanodes modified with different thickness of AlO_x layer at 1.23 V vs. RHE under AM 1.5G simulated sunlight at 100 mW cm^{-2} in the 1 M NaOH aqueous solution (pH = 13.6). b) Current-potential curves of Ta_3N_5, Ta_3N_5-AlO_x-25 photoanodes at 1.23V vs. RHE under AM 1.5G simulated sunlight at 100 mW cm^{-2} in the 1 M NaOH aqueous solution (pH = 13.6).

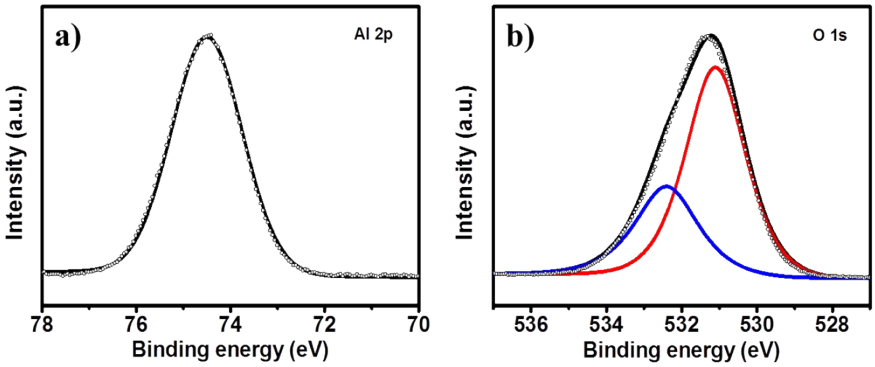

Fig. S2 a) XPS spectra of Al 2p for Ta_3N_5-AlO_x photoanode. b) XPS spectra of O 1s for Ta_3N_5-AlO_x photoanode.

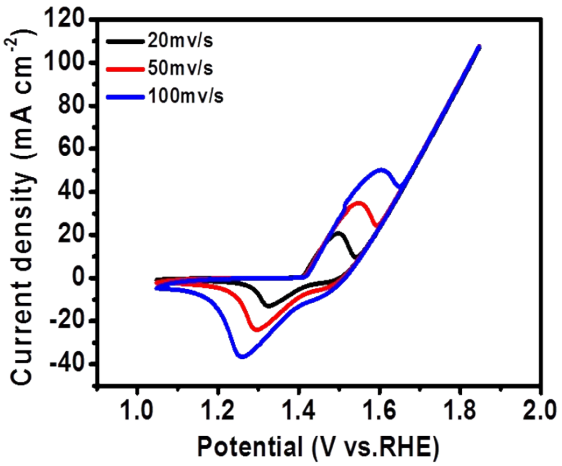

Fig. S3 Cyclic voltammogram measurements for $NiFeO_x$ cocatalyst on FTO under scan rates of 20, 50, 100 mV s^{-1} in 1 M NaOH aqueous solution (pH = 13.6).

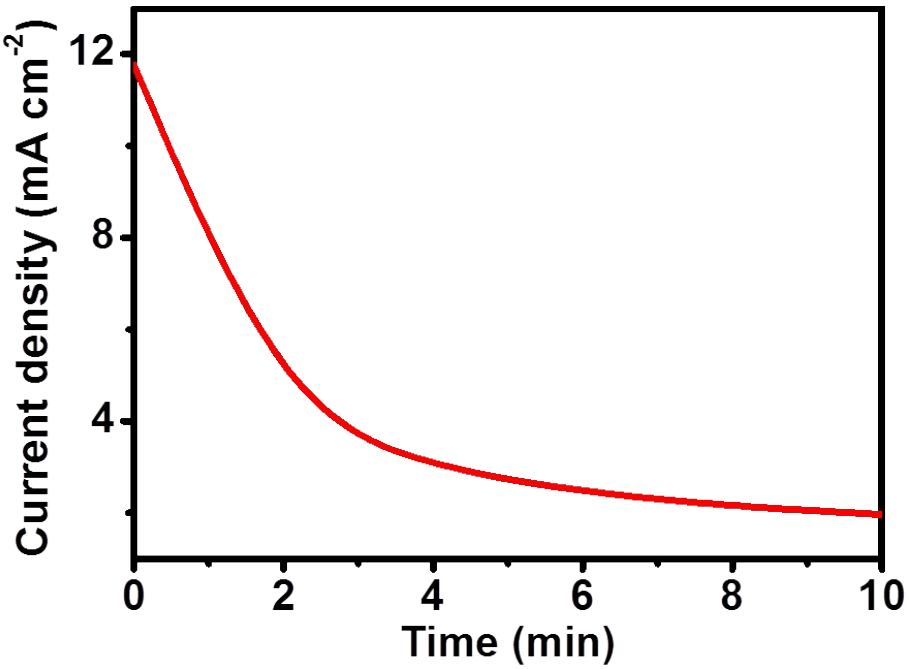

Fig. S4 Chronoamperometry measurement of Ta_3N_5-AlO_x-Fh-$NiFeO_x$ photoanode under AM 1.5G simulated sunlight at 1.23V in 1 M NaOH aqueous solution (pH = 13.6).

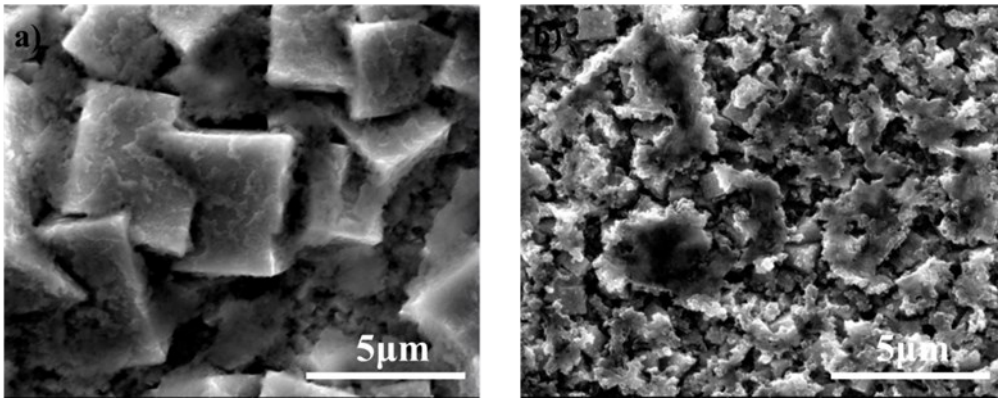

Fig. S5 a) The SEM image of Ta_3N_5-AlO_x-Fh-$NiFeO_x$ photoanode. b) The SEM image of Ta_3N_5-AlO_x-Fh-$NiFeO_x$ photoanode after stability test for 10min.

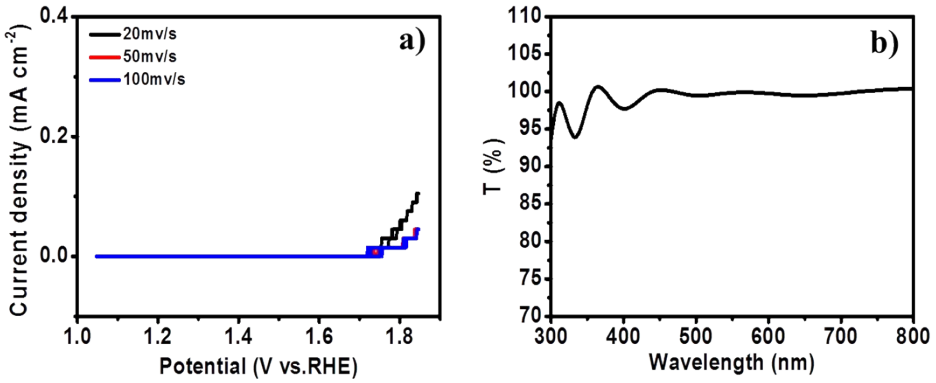

Fig. S6 a) Cyclic voltammogram measurements for CeO_x film on FTO under scan rates of 20, 50, 100 mVs^{-1}. b) Light transmittance test for CeO_x film on FTO.

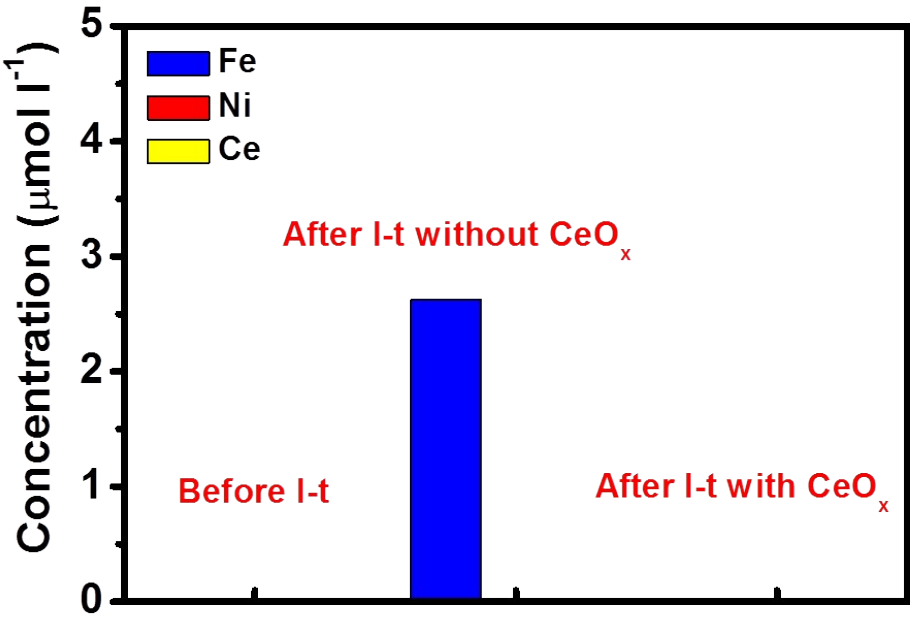

Fig. S7 ICP-OES analysis of NaOH solution before and after J-t measurement.

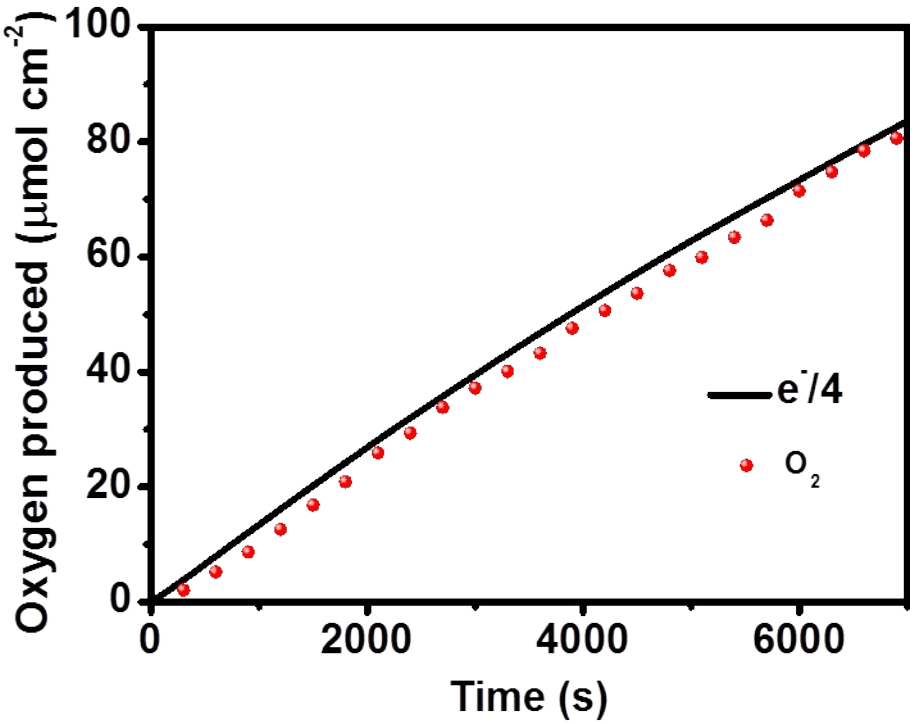

Fig. S8 Oxygen evolution measurement of the Ta_3N_5-AlO_x-Fh-$NiFeO_x$-CeO_x photoanode at 1.23 V in 1 M NaOH aqueous solution (pH = 13.6).

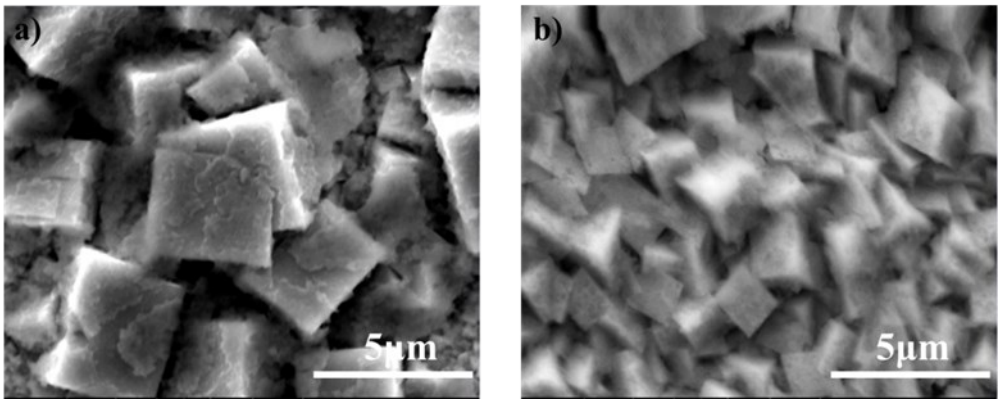

Fig. S9 a) The SEM image of Ta_3N_5-AlO_x-Fh-$NiFeO_x$-CeO_x photoanode. b) The SEM image of Ta_3N_5-AlO_x-Fh-$NiFeO_x$-CeO_x photoanode after stability test for 120 hours.

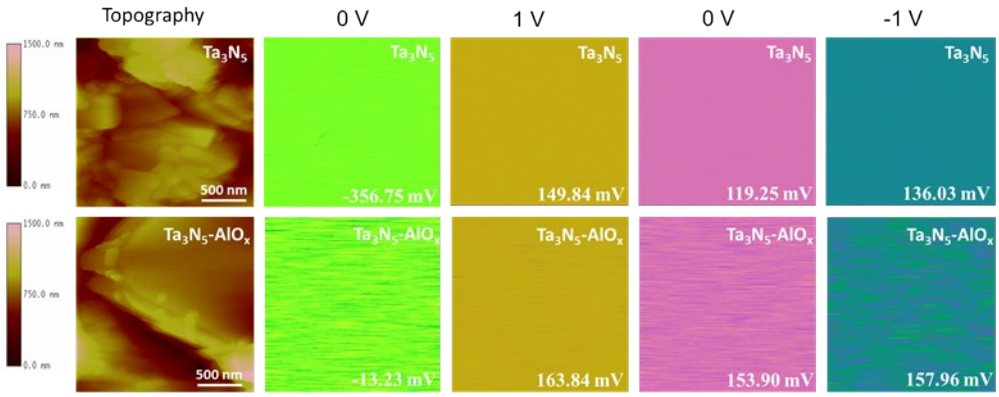

Fig. S10 Topography and CPD map of the Ta_3N_5 and Ta_3N_5-AlO_x photoanodes with different bias voltage in the dark.

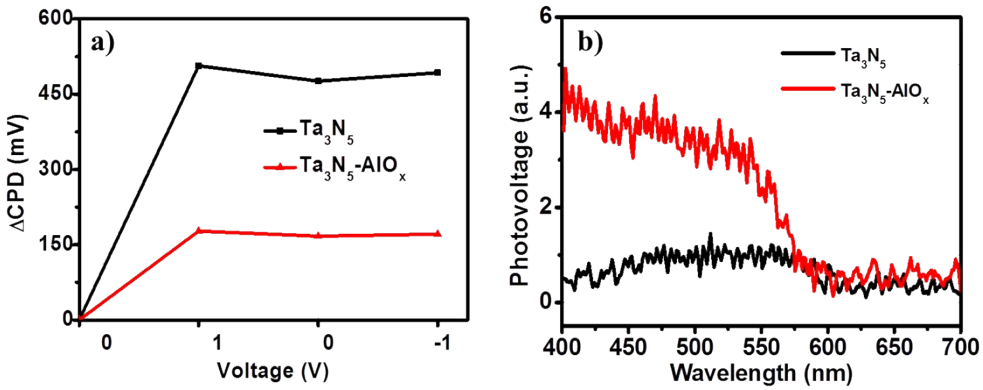

Fig. S11 a) Δ CPD values as a function of bias voltage applied to the tip. b) SPV responses of Ta_3N_5, Ta_3N_5-AlO_x photoanodes.

Kelvin probe force microscopy was also performed to further clarify the role of AlO_x layer. Different bias voltage of -1, 0, and 1 V were applied at the atomic force microscopy (AFM) tip in dark (Fig. S7) and contact potential difference (CPD) can be detected. Fig. S11a shows ΔCPD value of the sample with AlO_x layer is significantly lower than that of reference sample by about 400 mV, which shows that the interface trap states can be passivated. ΔCPD increased for both the samples at a bias of +1 V and -1 V, but the change rate is higher for control samples. In addition, ΔCPD value tends to be saturated after AlO_x layer modification, rather than fluctuating obviously with bis voltage changes. This indicates that the trap states of samples seem to be less sensitive to the electric field with AlO_x dielelctric layer. Accordingly, the AlO_x dielectric layer can effectively passivate trap states of Ta_3N_5 photoanode, which corresponds to the result in Fig. 3. This also confirmed by surface photovoltage spectroscopy (SPV) measurement results. As shown in Fig. S11b, the SPV response of Ta_3N_5-AlO_x photoanode is significantly higher than that of pristine one.

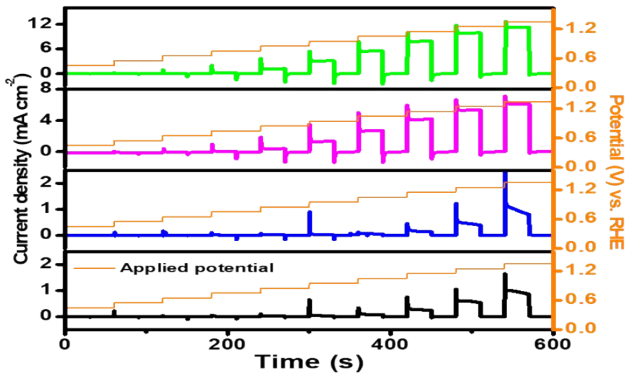

Fig. S12 Chopped light chronoamperometry measurements of Ta_3N_5 (black curve), Ta_3N_5-AlO_x (blue curve), Ta_3N_5-Fh (pink curve), Ta_3N_5-AlO_x-Fh (green curve) photoanodes in the 1 M NaOH aqueous solution (pH = 13.6). The potential is scanned from 0.45 to 1.45 V vs. RHE with a 0.1 V step and with a 60 s light on/off cycle on each step.

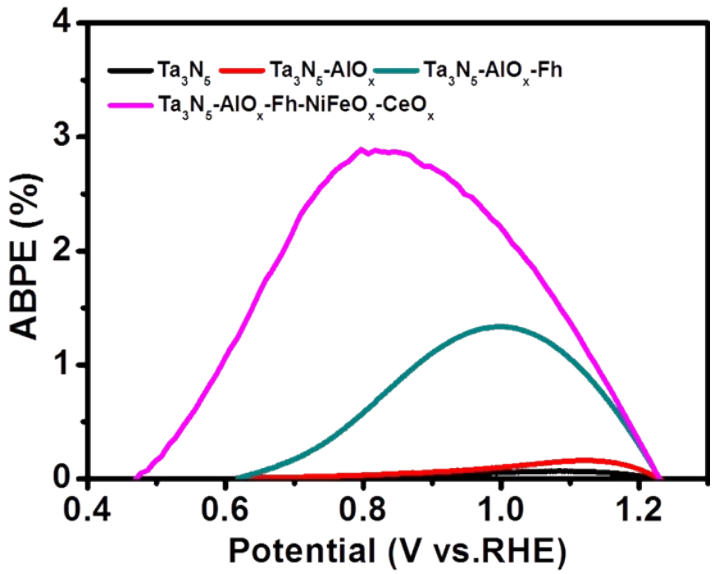

Fig. S13 The applied bias photon-to-current efficiency (ABPE) of Ta_3N_5, Ta_3N_5-AlO_x, Ta_3N_5-AlO_x-Fh, Ta_3N_5-AlO_x-Fh-$NiFeO_x$-CeO_x photoanodes.

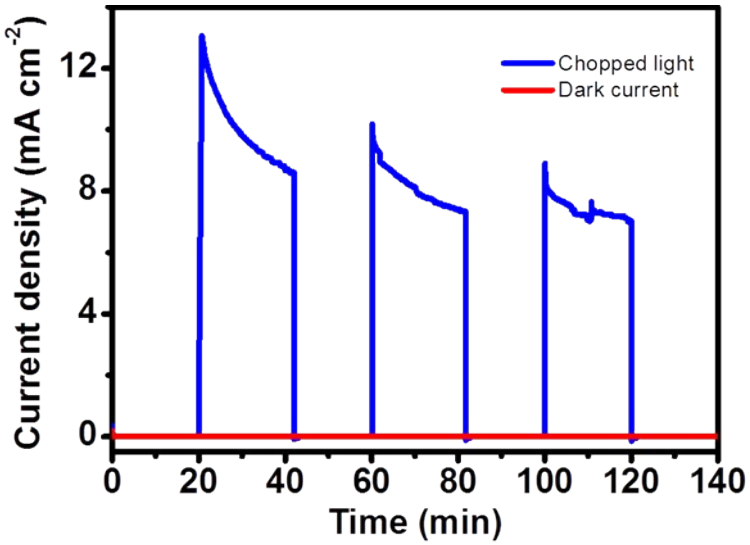

Fig. S14 The corresponding dark current and chopped light chronoamperometry measurement of Ta_3N_5-AlO_x-Fh-$NiFeO_x$-CeO_x at 1.23 V in 1 M NaOH solution.

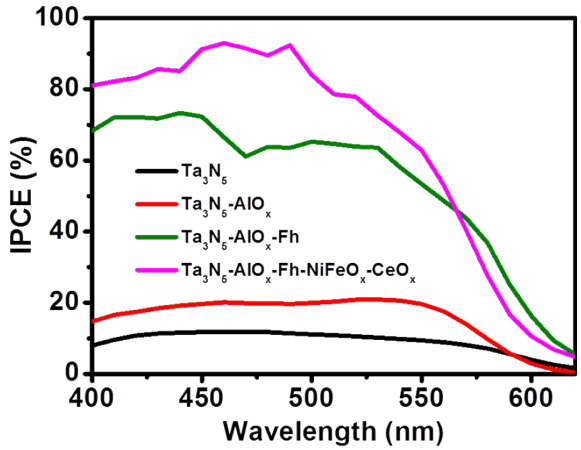

Fig. S15 IPCE curves of Ta_3N_5, Ta_3N_5-AlO_x, Ta_3N_5-AlO_x-Fh, Ta_3N_5-AlO_x-Fh-$NiFeO_x$-CeO_x photoanodes at 1.23 V in 1 M NaOH solution.

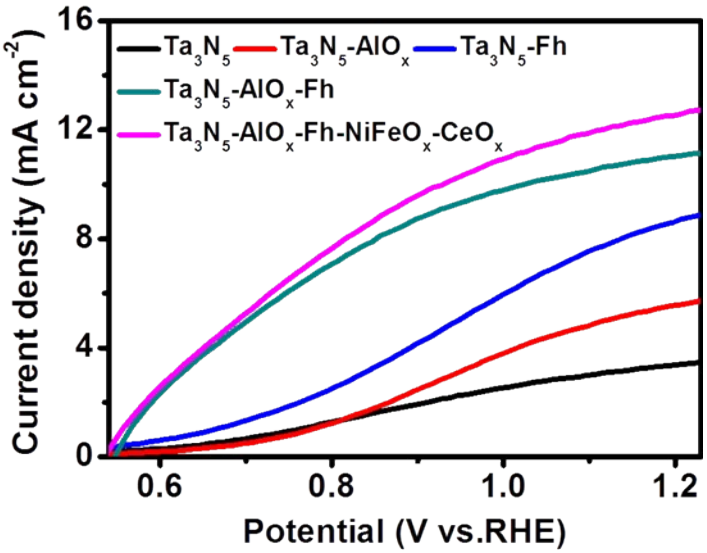

Fig. S16 Current-potential curves of Ta_3N_5, Ta_3N_5-AlO_x, Ta_3N_5-Fh, Ta_3N_5-AlO_x-Fh, Ta_3N_5-AlO_x-Fh-$NiFeO_x$-CeO_x photoanodes in 1 M NaOH-0.5M H_2O_2 solution.

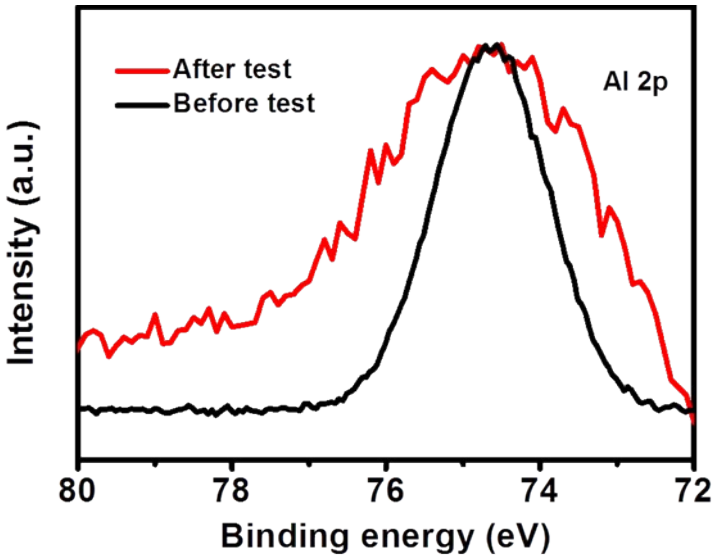

Fig. S17 XPS spectra of Al 2p for Ta_3N_5-AlO_x photoanode through oxygen production test.

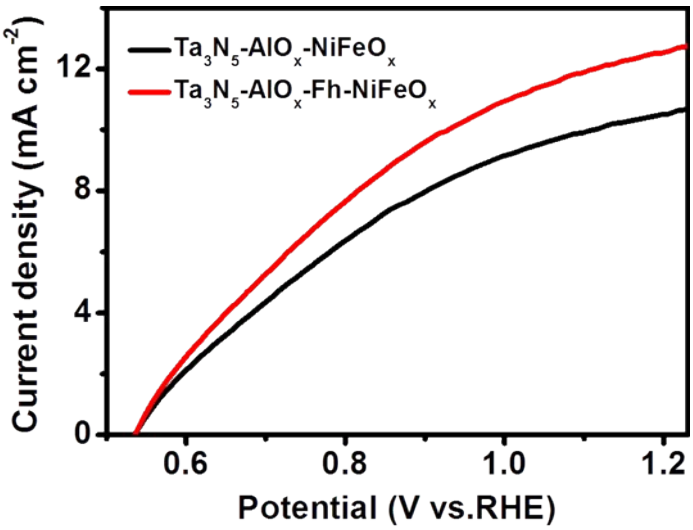

Fig. S18 Current-potential curves of Ta_3N_5-AlO_x-$NiFeO_x$, Ta_3N_5-AlO_x-Fh-$NiFeO_x$ photoanodes in 1 M NaOH-0.5M H_2O_2 solution.

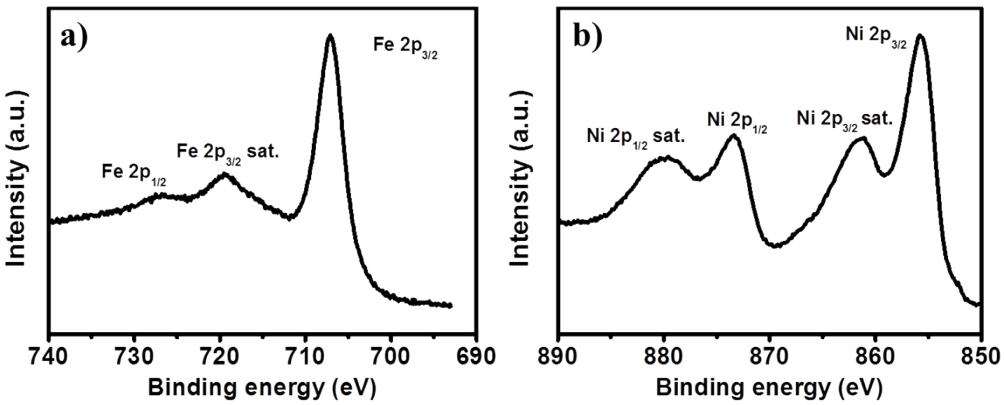

Fig. S19 XPS spectra of Fe 2p and Ni 2p for $NiFeO_x$.

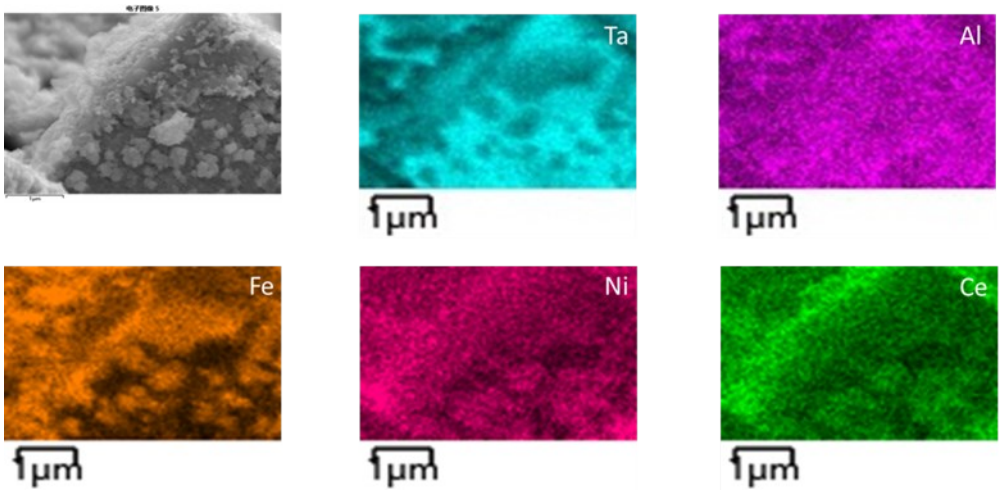

Fig. S20 The high-resolution cross section SEM characterizations with EDX mapping of the Ta_3N_5-AlO_x-Fh-$NiFeO_x$-CeO_x photoanode.

Table S1 Representative Ta_3N_5 based photoanode systems

Photoanode	J (mA cm^{-2}) at 1.23 V	ABPE (%)	Stability (h)	Ref.
Ba-Ta_3N_5/Co-Pi	6.7	1.5	0.5	1
Ta_3N_5/TiO_x/Fh/$Ni(OH)_x$/complex 1&2	12.1	2.5	0.5	2
Ta_3N_5-NR/$FeNiO_x$	9.95	2.72	1	3
gradient-Mg: Ta_3N_5/NiCoFe-Bi	8.5	3.31	5	4
Ta_3N_5/AlO_x/Fh/$NiFeO_x$/CeO_x	11.8	2.9	120	This work

References

1 Y. Li, L. Zhang, A. Torres-Pardo, et al. Nature Communications, 2013, 4, 2566.
2 G. Liu, S. Ye; P. Yan, et al. Energy & Environmental Science, 2016, 9, 1327.
3 Y. Pihosh, T. Minegishi, V. Nandal, et al. Energy & Environmental Science, 2020, 5, 1519.
4 Y. Xiao, C. Feng, J. Fu, et al. Nature Catalysis, 2020, 3, 932.